



HAL
open science

56 Gbps externally modulated widely tunable lasers with SOA boosters heterogeneously integrated on silicon

Amin Souleiman, Delphine Neel, Claire Besancon, Nicolas Vaissiere, Stephane Malhouitre, Karim Hassan, Jean Decobert, David Bitauld, Badr-Eddine Benkelfat, Kamel Merghem, et al.

► To cite this version:

Amin Souleiman, Delphine Neel, Claire Besancon, Nicolas Vaissiere, Stephane Malhouitre, et al.. 56 Gbps externally modulated widely tunable lasers with SOA boosters heterogeneously integrated on silicon. *Optics Express*, 2024, 32 (21), pp.37036-37045. 10.1364/OE.533266 . hal-04675644

HAL Id: hal-04675644

<https://hal.science/hal-04675644v1>


Submitted on 16 Dec 2024

HAL is a multi-disciplinary open access archive for the deposit and dissemination of scientific research documents, whether they are published or not. The documents may come from teaching and research institutions in France or abroad, or from public or private research centers.

L'archive ouverte pluridisciplinaire **HAL**, est destinée au dépôt et à la diffusion de documents scientifiques de niveau recherche, publiés ou non, émanant des établissements d'enseignement et de recherche français ou étrangers, des laboratoires publics ou privés.



56 Gbps externally modulated widely tunable lasers with SOA boosters heterogeneously integrated on silicon

A. SOULEIMAN,^{1,2} D. NEEL,¹ C. BESANCON,¹ N. VAISSIERE,¹
S. MALHOITRE,³ K. HASSAN,³  J. DECOBERT,¹ D. BITAULD,¹
B. BENKELFAT,² K. MERGHEM,² AND J. M. RAMIREZ^{1,*}

¹III-V Lab, a joint lab of Nokia, Thales and CEA, av. A. Fresnel, 91767 Palaiseau Cedex, France

²SAMOVAR, Télécom SudParis, Institut Polytechnique de Paris, 91120, Palaiseau, France

³CEA-Leti, Université Grenoble Alpes, F-38000 Grenoble, France

*amin.souleiman@3-5lab.fr

Abstract: We demonstrate externally modulated widely tunable lasers co-integrated with semiconductor optical amplifiers (SOAs) heterogeneously integrated on silicon. The widely tunable laser enables continuous single-mode operation over a tuning range of approximately 40 nm, with a side-mode suppression ratio (SMSR) of at least 50 dB and an average waveguide-coupled optical power of 5 mW. The integrated electro-absorption modulator (EAM) exhibits an extinction ratio (ER) of 16 dB when reversed biased at -2 V. The bit-error-rate (BER) measurements conducted across the available optical bandwidth (15 nm) showcase error-free transmission at 32 Gbps using non-return-to-zero (NRZ) signals for the majority of wavelengths in a back-to-back (B2B) configuration. Additionally, transmission measurements over distances of up to 10 km through a standard single-mode fiber (SSMF) have been successfully demonstrated. Dynamic extinction ratio (DER) values exceeding 4.5 dB are achieved for all wavelengths. Open-eye diagrams were measured up to 56 Gbps. These results demonstrate that this compact mono-epitaxial externally modulated tunable laser with integrated optical amplification can be a cost-effective transmitter solution for dense wavelength division multiplexing (DWDM) metropolitan and access networks.

© 2024 Optica Publishing Group under the terms of the [Optica Open Access Publishing Agreement](#)

1. Introduction

To reconcile high modulation speed, compactness, and low power consumption, externally-modulated transmitters represent a promising source for high capacity optical networks [1,2]. For achieving optical data encoding, III-V Electro-absorption modulators (EAMs) exploiting the quantum-confined Stark effect (QCSE) are good candidates since they offer compactness, high modulation efficiency, easy driving schemes and low energy consumption. Compared to Mach-Zehnder modulators (MZM), the EAMs operate at lower driving voltages, do not need complex segmented travelling wave electrode engineering and have lower insertion loss [3,4]. To realize such devices, various integration schemes, such as butt-joint integration (BJR) [5], selective area growth (SAG) [6,7], and quantum well intermixing (QWI) [8], have been used to achieve stable, reliable, and efficient externally modulated lasers (EMLs). However, these methods require sophisticated process control and have to face a higher fabrication cost driven by the III-V regrowth. In order to simplify device fabrication complexity and reduce cost, the use of the same active layer stack based on multiple quantum wells has been proposed for the laser, the EAM and the SOA device [9–11].

In this line, the use of a scalable technology becomes key to reduce the cost-per-chip even more. Thus, the integration of III-V materials on silicon photonics at wafer-scale to develop high-speed transceivers offers significant advantages over competing platforms. By leveraging

advanced and mature CMOS fabrication facilities, III-V-on-Si photonic integrated circuits (PICs) can be manufactured on 200 and 300 mm wafers with mass production capability [12]. Moreover, fabricated PICs can take advantage of the wafer-scale testing and packaging solutions developed by the silicon photonics community [13]. Several demonstrations of externally modulated transmitters have already been realized on the Si photonics platform. T. Hiraki and co-authors demonstrated in 2021 a high-speed membrane EAM on a Si platform that shows an on-chip loss lower than 4 dB at a wavelengths over 1590 nm and temperatures from 25 to 50°C [14]. An electro-optical bandwidth (EOBW) of 50 GHz was measured and open eye diagrams were obtained for 56 Gbps in non-return-to-zero on-off keying (NRZ-OOK) modulation and 112 Gbps when using four-level pulsed amplitude modulation (PAM4) signals. Later on, they also demonstrated a complete transmitter in the O-band by integrating a DFB laser with the EAM, obtaining over 67 GHz EOBW and a fiber-coupled output power of -2 dBm [15]. An externally-modulated widely tunable transmitter was demonstrated in Ref. [16], in which the micro-transfer-printing technology was used to integrate a tunable laser with a Si Mach-Zehnder modulator (MZM), showing 40 Gbps NRZ-OOK modulation in a back-to-back (B2B) configuration at wavelengths ranging from 1539 to 1573 nm with a fiber-coupled average power of -9 dBm and a threshold current around of 100 mA. III-V-on-Si transmitters are often integrated with on-chip SOAs to increase the optical power [17,18]. We previously reported an O-band EML-SOA module operating at 25 Gbps in NRZ with on-chip power of about 0 dBm [19]. In this paper, we demonstrate an externally-modulated widely tunable laser co-integrated with an SOA booster that operates at 56 Gbps in NRZ and delivers an on-chip output power up to 5 mW. The transmitter has an optical bandwidth of 15 nm, for wavelengths ranging from 1542 to 1557 nm and exhibits a dynamic extinction ratio (DER) of more than 4.5 dB for all wavelengths. We demonstrate bit-error-rate (BER) measurements at 32 Gbps in an error-free transmission in B2B configuration and up to 10 km transmission through standard single-mode fiber (SSMF).

2. Device fabrication and experimental setup

Figure 1 shows a picture of the finalized III-V-on-Si wafer (3 inches) with a zoomed view that depicts a simplified 3D schematic of the heterogeneously integrated III-V-on-Si transmitter co-integrated with an EAM and an SOA. Since we have used direct wafer bonding to define the III-V-on-Si platform, all three co-integrated components utilize the same III-V epitaxial stack. For this work, we have bonded a 3-inch III-V wafer on a 12-inch Si wafer. Such bonding technique has been used in a new generation of high-speed Si-based transceivers that show very convincing performance and maturity for the deployment in data centers [20]. Nevertheless, it also presents some constrains, especially when integrating different components closely spaced in a single waveguide that need a different III-V epitaxial stack for optimum performance, as is the case for this work. In spite of that, we can still find a good trade-off and use a single III-V epitaxy to demonstrate on-chip transmitters that account for a good optical power and a low driving voltage while enabling high-speed operation and a good extinction ratio (ER), as we will see here after. The heterogeneous III-V-on-SOI platform enables the fabrication of active components that propagate a hybrid mode that is confined in an electrically injected III-V waveguide and a passive Si waveguide simultaneously. The SOI platform contains a 500 nm crystalline Si layer and has a 2 μm buried oxide (BOX). The wafer is then etched to define two different Si waveguide heights, 300 nm for the Vernier filters, the Sagnac mirrors and the vertical grating couplers and 500 nm for the Si waveguide interposers located below the III-V waveguides to enable an efficient optical mode transfer. In contrast, the III-V epitaxial structure consists of multiple layers, including a PIN junction composed of P-doped InP, an AlGaInAs multi-quantum well (MQW) active region flanked by separated confinement heterostructures (SCH), and an N-doped InP layer. These InP-based layers are grown using metal organic chemical vapor phase epitaxy (MOVPE). The III-V active waveguides are defined after direct bonding of III-V epitaxial layers

onto a pre-patterned SOI wafer, followed by device metallization. A DVS-benzocyclobutene (BCB) passivation cladding ensures superior lateral optical confinement and avoids the lateral current leakage under high injection. This configuration offers an effective mode confinement in the QWs, resulting in reduced laser threshold current and an efficient optical modulation amplitude (OMA) [17]. Devices were fabricated following the process flow described in [21]. To compensate for the insertion loss introduced by the modulator as well as to provide further optical amplification, SOAs can be integrated at the outputs of the transmitters. A vertical grating coupler integrated at the SOA's output is used to enable wafer-level testing using optical fibers (see the SEM image in Fig. 1). To facilitate the optical mode transfer between devices (laser, EAM, and SOA), adiabatic couplers are typically employed to transition the optical signal from the III-V waveguide to the silicon waveguide. However, in this transmitter, the optical mode remains confined within the III-V waveguide, eliminating the need for couplers. This results in reduced parasitic capacitance, increased bandwidth, and a more compact footprint. Devices are electrically isolated by using an ion implantation followed by etching of the InGaAs p-contact (see the SEM image in Fig. 1). The double-pass ring-based Vernier filters are designed with two racetrack resonators coupled to a bus waveguide, each with respective free spectral ranges (FSR) of 2.52 nm and 2.68 nm, which provides a Vernier's FSR of 43.56 nm. The transmission coefficient between the bus waveguide and a single ring is ~ 0.93 . This parameter defines the ratio between the transmitted and incident field in the bus waveguide. Optical feedback in the tunable laser cavity is provided by a Bragg mirror (length = 12 μm and period = 242 nm) etched into a Si rib waveguide at the laser's output (20% of reflection) and a Sagnac mirror at the laser's backside (100% of reflection). Both components are shown in the SEM images of Fig. 1. For the EAM, we have a length of $L = 100 \mu\text{m}$ and an optical confinement of $\Gamma_{\text{QWs}} = 13.7\%$, while for the SOA, we have $L = 920 \mu\text{m}$ and a lower Γ_{QWs} of 10.95% to increase the output saturation optical power. For the laser, we have $L = 670 \mu\text{m}$, $\Gamma_{\text{QWs}} = 13.5\%$ and $\Gamma_{\text{bragg}} = 0.19\%$. These parameters provide a good trade-off that enables efficient operation of the laser, the EAM and the SOA simultaneously.

The experimental setup for evaluating the dynamic characteristics of the externally-modulated widely tunable laser co-integrated with the SOA booster (device under test, DUT) is illustrated in Fig. 2. The device is mounted on a stage equipped with a thermo-electric cooler (TEC) for temperature stabilization. To drive the transmitter module, a standard electrical source (Keithley 2400) is used along with either an RF signal for small signal analysis or with a pseudorandom binary sequence (PRBS) generator, connected to a two-stage variable-gain RF-linear amplifier (SHF S807 C) with a wide bandwidth. The optical signal generated is collected at the SOA side from the vertical grating coupler using a lensed optical fiber to minimize back-reflections. To prevent optical feedback from the setup, an optical isolator is included. An optical switch (1×4) facilitates the selection of different optical paths. The first path is connected to a power meter and an optical spectrum analyzer to evaluate the static performance. The second output signal is used to investigate the small-signal modulation response. This is achieved by applying a DC bias current and a low-amplitude RF signal generated by a vector network analyzer (VNA), and then analyzing the output power using an optoelectronic converter (Lightwave Component Analyzer, LCA Agilent N5242A/N4375B). The third optical path in the setup is utilized for transmission measurements. The output is connected to an EDFA (erbium-doped fiber amplifier) and a tunable bandpass filter (TBPF) to amplify and filter the received signal accordingly. On the receiver side, a high-speed photodiode (XPDV-2320R) is used. The amplified signal is sampled by a high-bandwidth Keysight storage oscilloscope with a bandwidth of 70 GHz (Agilent 86118A). The final path is designated for bit error rate (BER) measurements using the Anritsu MP1800A Signal Quality Analyzer, a multi-channel bit error rate tester (BERT). The signal is first amplified and filtered before passing through a variable optical attenuator (VOA) (Agilent 81577A) and a high-speed photodiode (XPDV-2320R) for these measurements. It is worth to mention that,

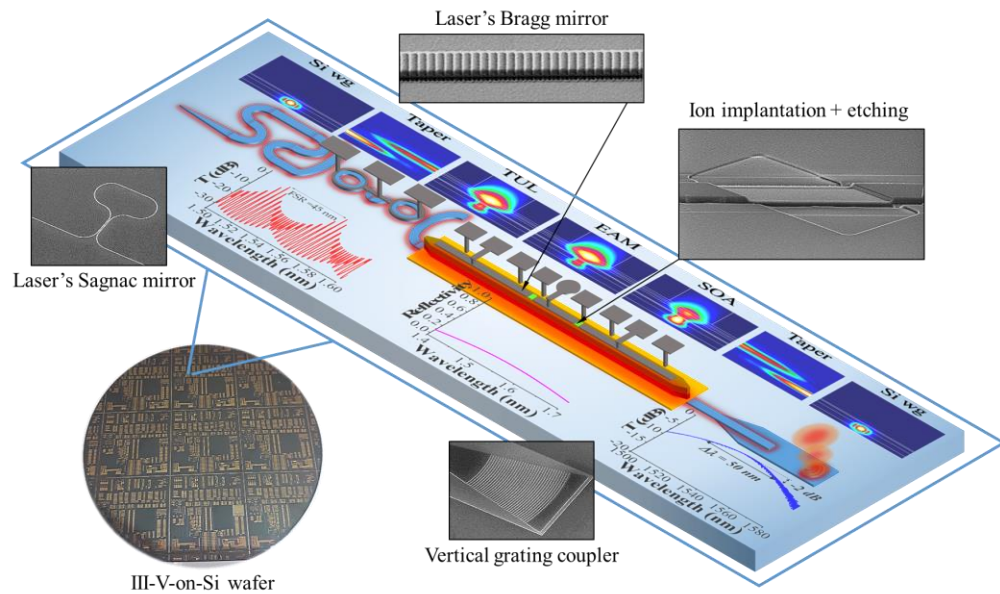


Fig. 1. Picture of the finalized wafer with a zoomed view showing the schematic structure of the heterogeneously integrated transmitter. From left to right: the highly reflective Sagnac mirror (SEM image); the Vernier filter; the III-V gain section of the laser; the low reflective laser's Bragg mirror (SEM image); the III-V section of the EAM and the SOA booster separated by electrically isolated areas (SEM image); and the fiber grating coupler (SEM image). The inset curves below show the simulated Vernier filter transmission for a wavelength range from $\lambda = 1500\text{--}1600$ nm and the simulated reflectivity and transmission spectrum of the Bragg mirror. The upper insets display several 2D FDM cross-section simulations of the TE optical mode for each component.

although we have not performed an in-depth yield analysis, the results presented here below are representative for several devices that have been measured at different sites of the wafer.

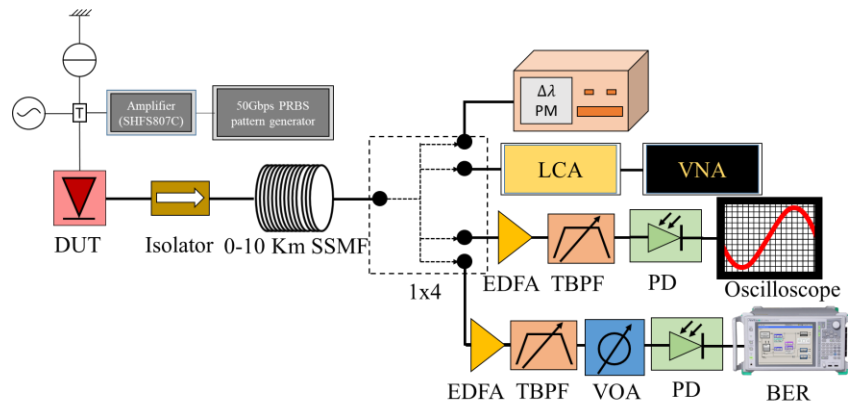


Fig. 2. Experimental setup used for the dynamic characterization of the DUT.

3. Static characterization

The widely tunable laser, EAM, and SOA co-integrated system were mounted on a temperature-controlled platform set at $T = 20^\circ\text{C}$. Figure 3(a) displays the on-chip output power as a function of the laser's injected current and for various values of injected current in the SOA when the EAM section is not biased. The output optical power is collected by a fiber grating coupler with a lensed fiber with a waist diameter of $3\ \mu\text{m}$, which introduces 3-4 dB of coupling losses. Several kinks in the L-I curve are observed, which we attribute to mode hopping due to the passive-active phase mismatch between the III-V gain section in the laser and the Vernier filter spectral response. A consistent increase in the L-I curve is observed for consecutive values of the injected current in the SOA, with a maximum of approximately 5 mW for an injected current of $I_{\text{SOA}} = 80\ \text{mA}$ in the SOA and for an injected current of $I_{\text{Laser}} = 100\ \text{mA}$ in the laser's gain section. Beyond this value of I_{SOA} , the optical power quickly saturates and steadily decreases for higher SOA current values, indicating the onset of nonlinear and/or thermal effects, as evident in Fig. 3(a) (see the red and orange curves). The measurements were performed for one laser emission wavelength around $\lambda = 1551\ \text{nm}$. In addition, a decrease of the laser's current threshold is observed for higher I_{SOA} values, which has been attributed to the optical feedback. Figure 3(b) represents the measured V-I response of the laser, from which we extracted a differential resistance of $7.5\ \Omega$ for $I_{\text{Laser}} = 100\ \text{mA}$, consistent with values reported elsewhere in similar devices [22,23]. In the inset, the V-I response of the thermal heaters is presented, showing a similar series resistance of approximately $R \approx 175\ \Omega$. Each thermal heater tunes the laser emission wavelength in steps of $\sim 2.7\ \text{nm}$ towards an opposite side of the spectral range, inducing a red shift (or a blue shift) to attain a total wavelength range of $\sim 40\ \text{nm}$.

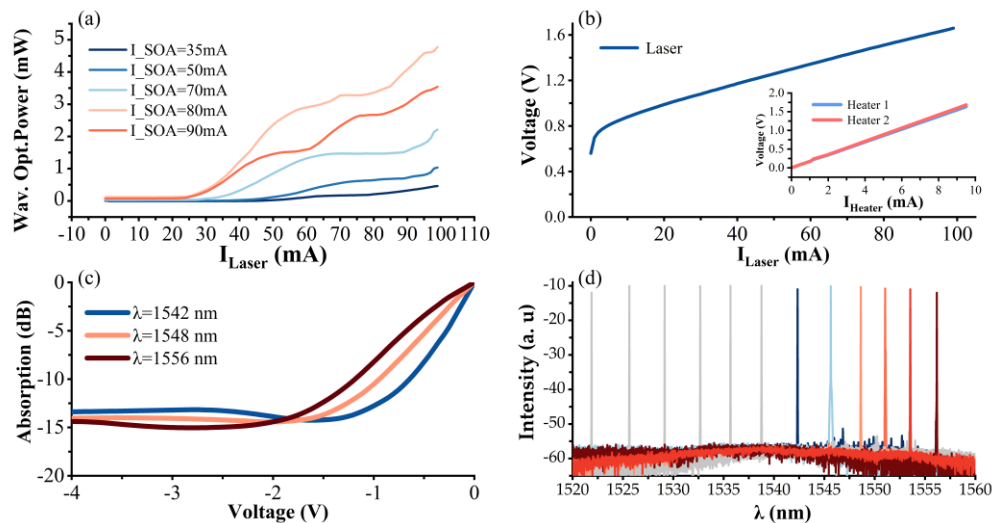


Fig. 3. (a) L-I characteristic of the tunable laser measured for different I_{SOA} values. (b) The measured V-I response of the laser and the thermal heaters (inset). (c) Measured optical absorption as a function of the reversed bias voltage in the EAM for different wavelengths. (d) Superimposed optical spectra for different operation modes in the widely tunable laser, showing the range of wavelengths in which the EAM can operate (coloured lines).

The static extinction ratio characteristic of the EAM has been explored. Illustrated in Fig. 3(c), the optical absorption of the EAM was measured at different wavelengths, varying with the applied reverse-bias voltage. Throughout the measurements, injection currents of 60 mA and 80 mA were maintained in the gain sections of the tunable laser and the SOA booster, respectively. Initially, the absorption increases steadily with the voltage until reaching saturation around -2 V,

indicating that the component has entered a regime of strong depletion. For longer wavelengths, a higher reverse bias is required to achieve the same optical absorption, suggesting that we are moving away from the modulator's absorption band edge, as expected. The maximum extinction ratio (ER) also varies with wavelength, peaking at 16 dB at 1556 nm and declining to 14.5 dB at 1542 nm. In Fig. 3(d), a superposition of the measured lasing spectra for different driving currents in the thermal heaters is presented. The gray spectra represent the laser wavelengths for which the EAM is not transparent in the off state. The colored spectra correspond to the range of wavelengths at which the EAM provides a good extinction ratio. The wavelength tuning range spans over 15 nm, from 1542 nm to 1557 nm. Throughout this range, a side-mode suppression ratio (SMSR) of at least ~ 50 dB is maintained.

4. Small signal analysis

Subsequently, we conducted a small signal frequency response measurement of the EAM using a vector network analyzer. The equipment was previously calibrated following the vendor's protocol. These measurements were performed at a single wavelength ($\lambda = 1551$ nm) and at a constant current of 80 mA for the SOA and 70 mA for the laser, at a temperature of 20°C. Figure 4 shows the EO bandwidth of the integrated EAM for the three available modulator lengths to assess the length's impact on bandwidth. All measurements were conducted with a bias voltage of -3 V. The gray curve shows the EO response of the high-speed photodiode (XPDV-2320R). We observed a very slow decay of the AM signal for all three EAMs, presumably due to an interface charge accumulation in the silicon substrate. The absence of a clear cut-off frequency, with a slope of at least -10 dB/decade, has conducted us to define the EOBW at -6 dB, as shown in the inset of Fig. 4. We observed a maximum bandwidth at approximately -3 V before saturation occurred. By reducing the modulator length from 200 μm to 100 μm , we nearly doubled the bandwidth, as expected. This resulted in an increase from 20 GHz for 200 μm to 38 GHz for 100 μm . A shorter modulator section has a lower RC constant, although it also reduces the extinction ratio. In our case, the measured ER for the most compact EAM ($L = 100$ μm) is good enough for 56 Gbps modulation, as it will be shown later on.

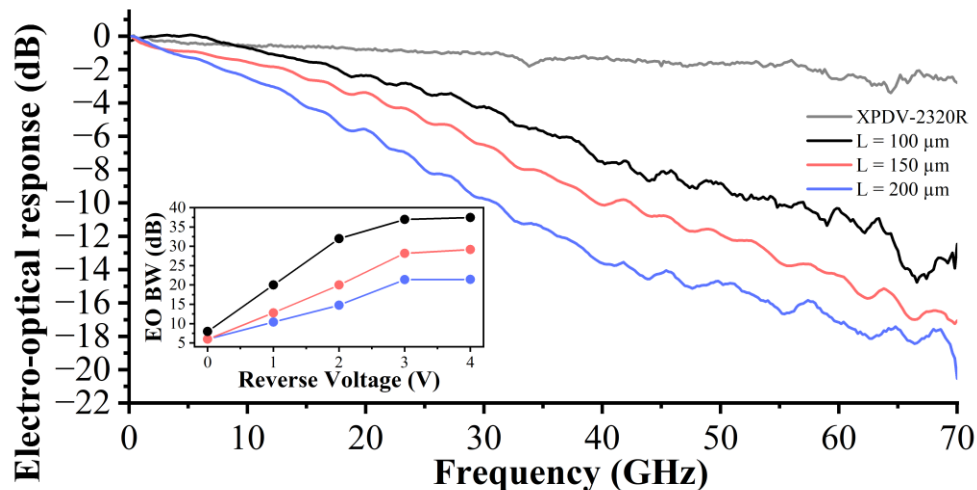


Fig. 4. Measured small-signal EO response for the high-speed photodiode used for the VNA calibration (gray curve) and for various lengths of the integrated EAM ($L = 100$ μm , 150 μm and 200 μm). The inset displays the measured EOBW at -6 dB as a function of the bias voltage.

5. Bit error rate and transmission measurements for 32-Gbps non-return-to-zero signals

The data transmission measurements were conducted at various wavelengths covering the entire optical bandwidth of the transmitter (~ 15 nm), with a step of ~ 3 nm (corresponding to the Vernier's coarse wavelength tuning), using 32 Gbps NRZ signals with a pattern length of $2^{31}-1$ at 20°C . The propagation distances span from 0 (B2B) to 10 km, with intervals of 2 km, employing standard single-mode fibers (SSMF). During the experiments, the current values in the gain sections of the laser, the SOA booster and the bias voltage of the EAM were slightly adjusted for each wavelength and distance to minimize the BER, remaining around 70 mA, 80 mA, and -2.5 V, respectively. The swing voltage (V_{pp} , peak-to-peak voltage) was fixed at 3 V for all measurements. The modulated waveguide-coupled output power varies between 2 and 3 mW in function of the transmitted wavelength. Figure 5 illustrates the obtained BER measurements after different transmission distances as a function of the received optical power at six different wavelengths: 1542 nm, 1545 nm, 1548 nm, 1551 nm, 1554 nm, and 1557 nm. The corresponding eye diagram can also be observed in the inset. We noted a decrease in the dynamic extinction ratio (DER) from 8.5 dB for the optimum transmission wavelength at $\lambda = 1554$ nm to 6.5 dB (for $\lambda = 1557$ nm) and 4.5 dB ($\lambda = 1542$ nm), which correspond to the wavelengths at each side of the transmitter's optical bandwidth. It is worth to remark that the optical bandwidth is limited, at the blue wavelength side of the optical spectrum, by the absorption band edge of the EAM (lower wavelength from which the EAM is transparent), and at the red wavelength side, by the longest attainable wavelength in the widely tunable laser, which is delimited by the optical gain wavelength span of the gain section. This fact can be easily observed by looking at the spectra of Fig. 3(d), where we can see that the lasing wavelength at $\lambda = 1557$ nm is almost at the band edge of the optical gain spectrum. Error-free propagation was achieved for most tested wavelengths in the B2B configuration and for transmission distances up to 2 km. Figure 5(e) depicts the measured BER and eye diagrams at a wavelength of 1554 nm. A negligible power penalty was observed when comparing the B2B measurement (dark blue) with the +2 km transmission (light blue). For B2B testing, a received power sensitivity of approximately -5.5 dBm was achieved

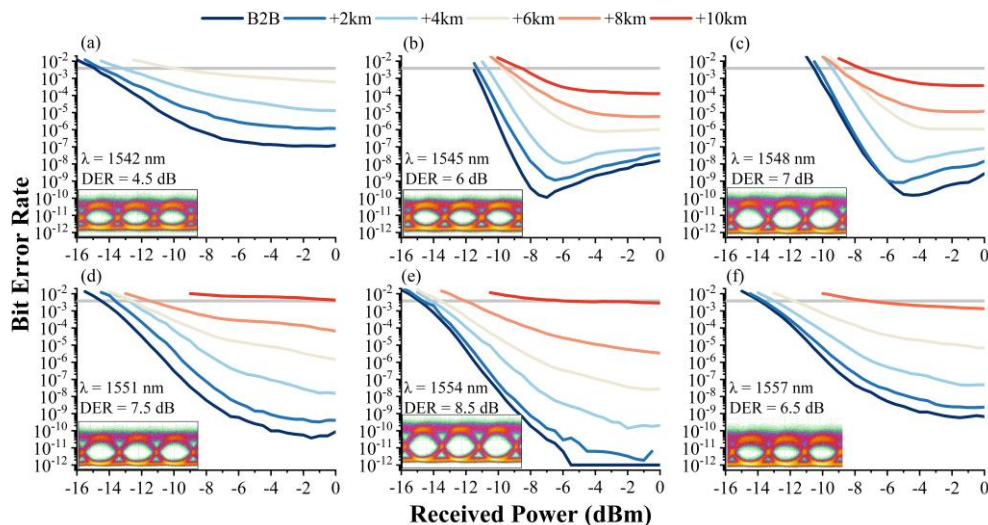


Fig. 5. Measured BER at 32 Gbps as a function of the received power for each wavelength over distances ranging from B2B to 10 km with a step of 2 km. The inset shows the eye diagrams for each wavelength, and the gray horizontal lines mark the HD-FEC limit.

for a BER of 10^{-12} , which corresponds to the minimum measurable value of our equipment. Notably, there was a power penalty of 0.5 dB, 1 dB, and 2.8 dB in the received optical power at the 7% HD-FEC limit, respectively, when compared with the 4 km, 6 km, and 8 km transmissions under B2B conditions. We observed increasing degradation with transmission distance, which can be attributed to a combination of optical feedback, loss, and chirp. Longer transmission distances are expected using optical links that partially compensate for chirp, such as non-zero dispersion shifted fibers (NZ-DSF).

The EAM and the SOA having opposite chirp values, a fine tuning of their driving voltage and current values enables for a partial compensation of the chirp, enabling longer transmission distances than in directly modulated lasers (DMLs) or externally modulated lasers without SOA boosters (EMLs) [24]. It is worth mentioning that, for all wavelengths, the power penalty is smaller than 0.5 dB at the 7% HD-FEC limit when comparing B2B transmission with the +2 km transmission, indicating good data transmission performance.

6. Transmission measurements for 50 Gbps and beyond

We evaluated the large-signal intensity modulation of the III-V/Si widely tunable transmitter through data transmission experiments using a NRZ-OOK signal with a $2^{31}-1$ PRBS pattern length. The DC bias current operating points for the tunable laser and the SOA section were established at 65 mA and 70 mA, respectively. The reverse bias voltage of the EAM is set at -2.5 V, while the swing voltage is fixed at 3 V for all measurements. Fig. 7(a) illustrates open eye diagrams for a B2B configuration at 1550 nm, demonstrating 50 Gbps modulation speed with a dynamic extinction ratio of 4.7 dB. Similar ER values were obtained for other wavelengths after optimization of the operating point for each device in the transmitter.

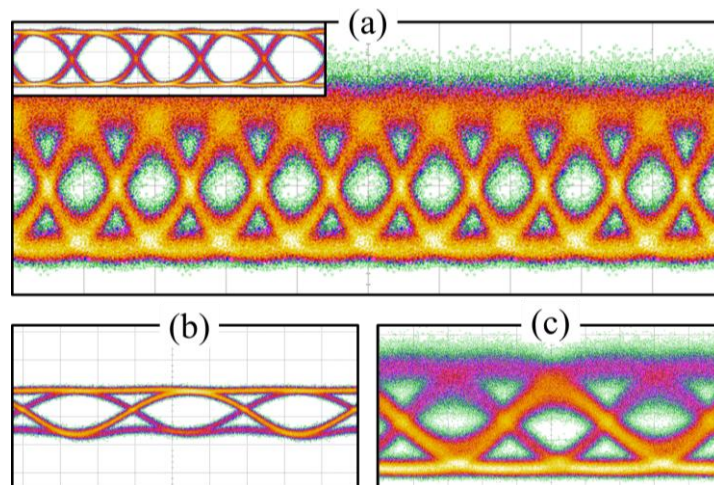


Fig. 6. Optical and electrical eye diagrams measured from an NRZ modulation signal with a PRBS pattern length of $2^{31}-1$ in a back-to-back configuration at different modulation speeds: (a) 50 Gbps, with the inset displaying the electrical eye diagrams. (b) and (c) showcase the electrical and optical eye diagrams for 56 Gbps.

At last, the 56 Gbps NRZ large signal modulation was conducted using a $2^{31}-1$ PRBS pattern length at the same wavelength. The swing voltage remains constant, and the bias voltage applied to the EAM is approximately -2.2 V. The bias current for the tunable laser and the SOA were set at 65 mA and 66.8 mA, respectively, representing the optimal values for measuring open eye diagrams at such bit rate. Figure 6(b) and 6(c) show the input electrical signal and the output optical eye diagrams respectively, which reveals a dynamic extinction ratio of 4 dB. The electrical

eye diagram starts showing distortion introduced by the RF amplifier, which shows a gradual performance degradation beyond 50 GHz. As a consequence, the optical eye diagram shows a slightly distorted signal with some jitter, although it still provides clearly discernible openings. It is worth to remark that we did not use any electrical amplification or post-data treatment at the receiver, nor equalization for all the measurements, which could significantly enhance the component's performance. Additionally, as the EAM modulator is an RC-limited device, further bandwidth enhancement can be achieved by reducing its length even more, although we will have an additional penalty on the extinction ratio. Still, this high-speed and widely tunable III-V/Si transmitter has shown good dynamical properties up to 56 Gbps in the C-band, providing a good starting point to develop high-speed and compact silicon photonic transmitters that can be used in high-capacity optical networks.

7. Conclusion

In this study, we demonstrated III-V-on-Si C-band transmitters based on externally-modulated widely tunable lasers with integrated semiconductor optical amplifiers. By using ring-based Vernier filters, the laser exhibits a wide single-mode wavelength tuning range of approximately 40 nm with stable monomode operation and an SMSR of at least 50 dB, achieving up to 5 mW of on-chip output power. Through static characterization, we investigated the performance of the EAM, revealing an extinction ratio that varies with wavelength, peaking at 16 dB at 1556 nm. Small signal analysis of the EAM demonstrated a 6 dB cut-off frequency bandwidth of 38 GHz. Bit-error-rate measurements confirmed error-free transmission at 32 Gbps in a B2B configuration for several wavelengths, and transmission over various distances was conducted with moderate power penalties, not exceeding 2.8 dB for a transmission of 8 km through SSMF. Furthermore, large-signal intensity modulation experiments demonstrated the transmitter's capability to achieve transmission rates of up to 56 Gbps non-return-to-zero with a dynamic extinction ratio of 4 dB in the eye diagram in a B2B configuration. These results underscore the potential of III-V/Si integrated transmitters for high-speed and compact silicon photonic applications, paving the way for future developments in wavelength division multiplexing applications.

Funding. European Union Horizon 2020 Framework Programme (H2020-ICT-2017-1).

Disclosures. The authors declare no conflicts of interest.

Data availability. Data underlying the results presented in this paper are not publicly available at this time but may be obtained from the authors upon reasonable request.

References

1. B. Schrenk, "Electroabsorption-modulated laser as optical transmitter and receiver: status and opportunities," *IET Optoelectron.* **14**(6), 374–385 (2020).
2. J. Yang, M. Tang, S. Chen, *et al.*, "From past to future: on-chip laser sources for photonic integrated circuits," *Light: Sci. Appl.* **12**(1), 16 (2023).
3. H.-W. Chen, Y. H. Kuo, and J. E. Bowers, "High speed silicon modulators," *2009 14th OptoElectronics and Communications Conference*, Hong Kong, China, 2009, pp. 1–2.
4. M. J. William, Michael J. Green, Rooks, *et al.*, "Ultra-compact, low RF power, 10 Gb/s silicon Mach-Zehnder modulator," *Opt. Express* **15**(25), 17106–17113 (2007).
5. W. Kobayashi, M. Arai, T. Yamanaka, *et al.*, "Design and fabrication of 10-/40-Gb/s, uncooled electroabsorption modulator integrated DFB laser with butt-joint structure," *J. Lightwave Technol.* **28**(1), 164–171 (2010).
6. J. Decobert, P.-Y. Lagr e, H. Guerault, *et al.*, "AlGaInAs selective area growth for high-speed EAM-based PIC sources," *2013 International Conference on Indium Phosphide and Related Materials (IPRM)*, Kobe, Japan, 2013, pp. 1–2.
7. J. Decobert, G. Binet, A. D. B. Maia, *et al.*, "AlGaInAs MOVPE selective area growth for photonic integrated circuits," *Adv. Opt. Techn* **4**(2), 167–177 (2015).
8. E. J. Skogen, J. W. Raring, G. B. Morrison, *et al.*, "Monolithically integrated active components: A quantum-well intermixing approach," *IEEE J. Select. Topics Quantum Electron.* **11**(2), 343–355 (2005).
9. L. Hou, M. Tan, M. Haji, *et al.*, "EML based on side-wall grating and identical epitaxial layer scheme," *IEEE Photonics Technol. Lett.* **25**(12), 1169–1172 (2013).

10. H. Klein, C. Bornholdt, G. Przyrembel, *et al.*, “40 Gbit/s identical layer InGaAlAs-MQW electroabsorption-modulated DFB-lasers operating between 1298 nm and 1311 nm,” in *Proceedings Indium Phosphide and Related Materials*, (Santa Barbara, USA), 2012.
11. Y. Xia, Q. Li, J. Meng, *et al.*, “25Gbps EA-modulated widely tunable V-cavity laser transmitter,” *IEEE Photon. Technol. Lett.* **36**(6), 385–388 (2024).
12. B. Szlag, K. Hassan, L. Adelmini, *et al.*, “Hybrid III-V/Silicon technology for laser integration on a 200-nm Fully CMOS-compatible silicon photonic platform,” *IEEE J. Select. Topics Quantum Electron.* **25**(5), 1–10 (2019).
13. C. Xiang, C. Xiang, S. M. Bowers, *et al.*, “Perspective on the future of silicon photonics and electronics,” *Appl. Phys. Lett.* **118**(22), 220501 (2021).
14. T. Hiraki, T. Aihara, Y. Maeda, *et al.*, “50-GHz-bandwidth membrane InGaAsP electro-absorption modulator on Si platform,” *J. Lightwave Technol.* **39**(16), 5300–5306 (2021).
15. T. Hiraki, A. Takuma, M. Yoshiho, *et al.*, “Over-67-GHz-bandwidth membrane InGaAlAs electro-absorption modulator integrated with DFB laser on Si platform,” *J. Lightwave Technol.* **41**(3), 880–887 (2023).
16. J. Zhang, E. Soltanian, B. Haq, *et al.*, “Integrated optical transmitter with micro-transfer-printed widely tunable III-V-on-Si laser,” in *Optical Fiber Communication Conference (OFC)* (Optica Publishing Group, 2022), p. Tu2D.2.
17. J. M. Ramírez, P. F. de la Horie, J. G. Provost, *et al.*, “Low-Threshold, High-Power On-Chip Tunable III-V/Si Lasers with Integrated Semiconductor Optical Amplifiers,” *Appl. Sci.* **11**(23), 11096 (2021).
18. R. Kumar, G. L. Su, D. Huang, *et al.*, “Fully Integrated Tunable III-V/Si Laser with On-chip SOA,” *J. Lightwave Technol.* **42**(9), 3314–3319 (2024).
19. L. Ghorbel, A. Gallet, A. Shen, *et al.*, “25Gb/s Error-free transmission with a packaged chipset integrating a III-V/SOI DFB laser, an electro-absorption modulator and a semiconductor optical amplifier,” in *IEEE 14th International Conference on Group IV Photonics* (2017).
20. X. Wang, R. Kumar, D. Huang, *et al.*, “16-channel integrated multi-wavelength DFB lasers with 200 GHz channel spacing,” in *Novel In-Plane Semiconductor Lasers XXIII* (Vol. 12905, pp. 99–104). SPIE, (2024, March).
21. J. M. Ramírez, A. Souleiman, P. F. de la Horie, *et al.*, “Low- κ , narrow linewidth III-V-on-SOI distributed feedback lasers with backside sampled Bragg gratings,” *Opt. Express* **30**(20), 36717–36726 (2022).
22. A. Souleiman, D. Néel, N. Vaissiere, *et al.*, “High-Speed Direct Modulation on III-V-on-SOI Distributed Feedback Lasers with Intrinsic Electro-Optical Bandwidth Over 20 GHz,” *2023 Conference on Lasers and Electro-Optics Europe & European Quantum Electronics Conference (CLEO/Europe-EQEC)*, Munich, Germany, 2023, pp. 1.
23. J. Zhang, L. Bogaert, C. Krückel, *et al.*, “Micro-transfer printing InP C-band SOAs on advanced silicon photonics platform for lossless MZI switch fabrics and high-speed integrated transmitters,” *Opt. Express* **31**(26), 42807–42821 (2023).
24. W. Kobayashi, M. Arai, T. Fujisawa, *et al.*, “Novel approach for chirp and output power compensation applied to a 40-Gbit/s EADFB laser integrated with a short SOA,” *Opt. Express* **23**(7), 9533–9542 (2015).